Near infrared integrated photonic switches for portable quantum sensors

Near infrared integrated photonic switches for portable quantum sensors

Bruce Saleeb-Mousa, James L. Moss, Jessica O. Maclean, Richard P. Campion and Christopher J. Mellor

School of Physics and Astronomy, University Park, The University of Nottingham, Nottingham, NG7 2RD, UK

E-mail: bruce.saleeb-mousa@nottingham.ac.uk

Abstract. A novel integrated semiconductor photonic switch, based on carrier-induced refractive index changes, has been designed and fabricated for use at near infrared wavelengths (890-920 nm, 750-780 nm and 745-775 nm). These switches are intended for use in quantum sensors which rely on the spectroscopy of caesium, rubidium or potassium atoms respectively. The beam-steering properties of the 890-920 nm device are presented and its extinction ratio measured to be 13.4 dB. This measurement was limited by coupling efficiency. Subsequent changes made to the testing equipment include the implementation of an automated testing routine. This new experimental setup will facilitate the full characterisation of the 890-920 nm device and the newly fabricated optical switches, designed for operation in the wavelength ranges 750-780 nm and 745-775 nm respectively.

1. Introduction

Wave-particle duality underpins the behaviour of cold atomic matter, opening up the possibility of performing atom interferometry. Such experiments have proven to be a powerful method of precision inertial sensing [1]. In particular, the cold-atom gravimeter has demonstrated itself to be a useful tool in obtaining precise values of the local gravitational acceleration, in the region of $\delta g/g = 10^{-9}$ [2], demonstrating long-term stability, and high accuracy. The promising performance of these atom interferometers lend themselves to applications in many areas of modern physics and engineering, such as tests for the equivalence principle [3], determination of fundamental constants such as the fine structure constant, α [4] and Newton's gravitational constant, G [5], geosurveys, and proposals for gravitational wave detection [6].

Recent research and investment in the field of quantum sensing and metrology in the UK [7], and around the world, has brought about a need for compact, integrated enabling technologies, with the aim of converting the next generation of quantum sensors from laboratory-based experiments to innovative and marketable products. This has led to an enhanced drive to develop these mainly laboratory-based systems towards more compact, low power, and portable equivalents [8]. For example, the European iSense project [9] used a cold atom gravimeter as a demonstrator and featured a micro-integrated laser system, fibre optical delivery system, compact vacuum system and atom chip assembly, all integrated in a transportable package weighing around 63 kg [10].

Since these sensors rely heavily on carefully tuned and timed laser pulses, reliable optical subsystems are required to deliver and manipulate such pulses. Further development of these sensors into a fully integrated package thus requires the optimisation of size, weight and power (SWaP), through miniaturisation of such optical subsystems into a single, compact and robust package. In particular, optical switching plays a crucial role in the operation of atom interferometry based quantum sensors, such as the quantum gravimeter - ensembles of atoms must be first trapped and cooled under vacuum using a magneto-optical trap (MOT). The MOT is then switched off and, since atom interferometry is based around the probabilistic nature of atomic transitions, light is used to manipulate matter waves, akin to the mirror and beamsplitter in a classical Mach-Zehnder Interferometer (MZI). The principle of conservation of momentum, upon interaction of the atoms with an electromagnetic field, is used to form an interferometry sequence. A common sequence of pulses is the scheme developed by Kasevich and Chu [11], consisting of three separate pulses. The first initiates the atoms in a coherent superposition of ground and excited states, the second inverts the population and the final pulse is used for recombination. Within this scheme, two different types of optical switching are required - fast switching ($\sim \mu$s), which is used for state preparation and the interferometry sequence, and high extinction ratio switching, used to ensure that the light from the MOT is not present during the formation of the interferometer, which would degrade the final signal. Typically, acousto-optical modulators (AOMs) are used for the fast switching and a combination of AOMs and mechanical beam shutters for the high extinction switching. Mechanical shutters offer very high extinction and are available in the form of low power, integrated compact packages, however, due to their mechanical nature, they do not offer sufficient switching speeds for interferometry sequences and furthermore can suffer from unwanted vibration-induced effects, such as switch 'bouncing', during the actuation of their mechanism [10]. AOMs can provide the fast switching speeds required, with most commercial devices capable of consistent switching speeds on the order of hundreds of nanoseconds or better. However, these devices rely on high power, high frequency ($\sim$1 W, $\sim$100 MHz) signals to operate, requiring additional components. Moreover, due to the nature of their operation, it is challenging to attain high extinction ratio switching ($>$ 80 dB) with these devices in smaller packages. This enhances the requirement for reliable and robust integrated optical subsystems, which match or surpass the performance of the technologies currently in use.

2. Optical Switch Design & Theory

The III-V semiconductor material system offers an attractive platform for integrated photonics since it allows monolithic integration of multiple devices, such as lasers, amplifiers, photodetectors, switches and waveguides on a single chip [12]. Furthermore, optical switches based on the III-V material system enable alternative switching mechanisms in addition to the commonly used electro-optic effect, such as carrier-induced refractive index change effects [13]. These effects facilitate manipulation of the local refractive index profile in the device to steer light into a desired output position. The proposed optical switch design exploits this using an $Al_xGa_{(1-x)}As/Al_yGa_{(1-y)}As$ heterostructure, where x and y are the fractional aluminium concentrations in the cladding and core layers respectively. An illustration of the switch design is shown in Figure 1.

The switch design consists of a heterostructure grown on semi-insulating (SI) GaAs using in-house molecular beam epitaxy (MBE). Standard photolithography and dry etching techniques are then used to form the device structure. Ohmic contacts are deposited using a thermal evaporation process. Layer thicknesses were chosen to ensure optimal optical and carrier confinement in the core, the latter determining the strength of the refractive index change due to the Moss-Burstein effect, also known as the band-filling effect [13]. The operation of the switch may be described as follows: at the cleaved facet light is coupled into the active steering region.

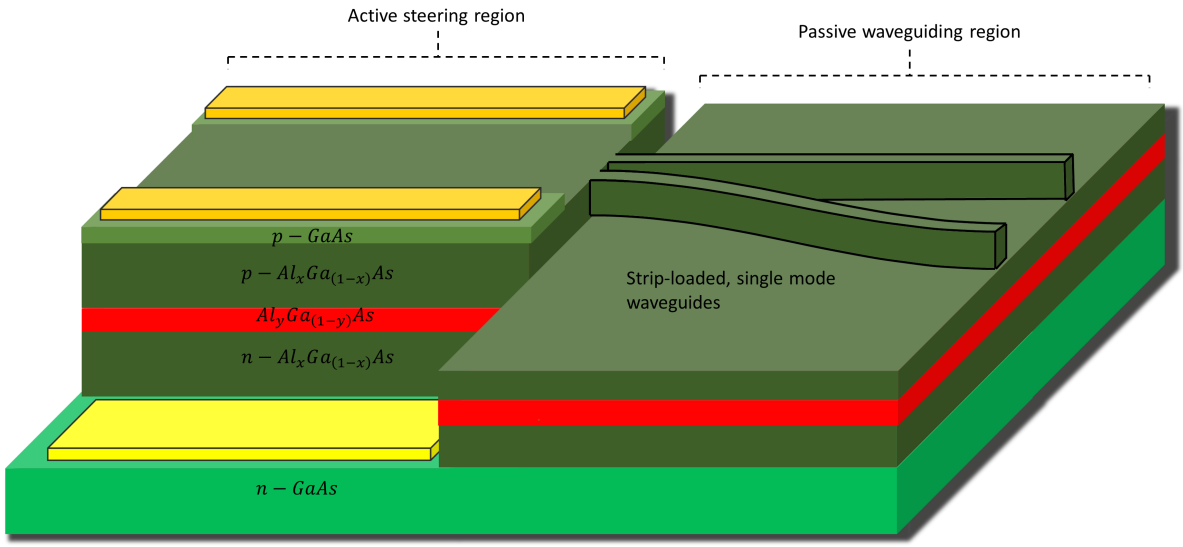

Figure 1. Illustration of the proposed switch design showing the various epitaxial layers, mesa structure and single mode strip-loaded waveguides.

A small voltage is applied across each set of contacts on either side of the mesa, causing an injection of carriers into the core layer, where they begin to diffuse. A portion of these carriers is lost by leakage effects. Those that are confined to the core cause a reduction in the band gap, followed by band-filling [13]. The result is an overall decrease in the local refractive index profile of the core under the contacts, as illustrated in Figure 2, forming a channel waveguide with a reduced effective index of refraction, n_{eff}, in this region. By changing the balance of the voltages between the contacts, the carrier profile in the core can be altered and consequently the refractive index profile, allowing the guided beam to be steered into one of the two output strip-loaded waveguides at the end of the steering region. For example, with balanced currents, light enters the input facet in between the two regions of depressed refractive index and subsequently propagates through the steering region by total internal reflection (TIR), akin to propagation through a graded index waveguide. The strip-loaded waveguides are used to provide confinement in both x and y (propagation in z), by partially etching away the top cladding layer [14]. Using this configuration, the beam may be switched on or off by steering into the straight or curved waveguide respectively. By cascading these devices in series on a single chip, i.e. the output channel of the first device becomes the input for the subsequent device, an enhanced extinction ratio may be achieved.

Three different epitaxial designs were proposed for switching light at the following near infrared (NIR) wavelengths: Sample A (890-920 nm), Sample B (750-780 nm) and Sample C (745-775 nm). These are intended for use in caesium, rubidium, or potassium based quantum sensors respectively. These designs were calculated to operate in the aforementioned wavelength regions by changing the aluminium concentration in the cladding and core, and the thicknesses of the layers to ensure minimal absorption and maximum confinement of the guided wave. This was achieved by first calculating the refractive index of the core and cladding layers separately according to [15], followed by calculation of the effective index of propagation using the effective index method [16]. The dimensions of the strip-loaded waveguides were also calculated to ensure propagation of only the fundamental TE_{00} mode. The output of the curved waveguide was displaced 250 μm laterally from the output of the straight waveguide to allow for standard

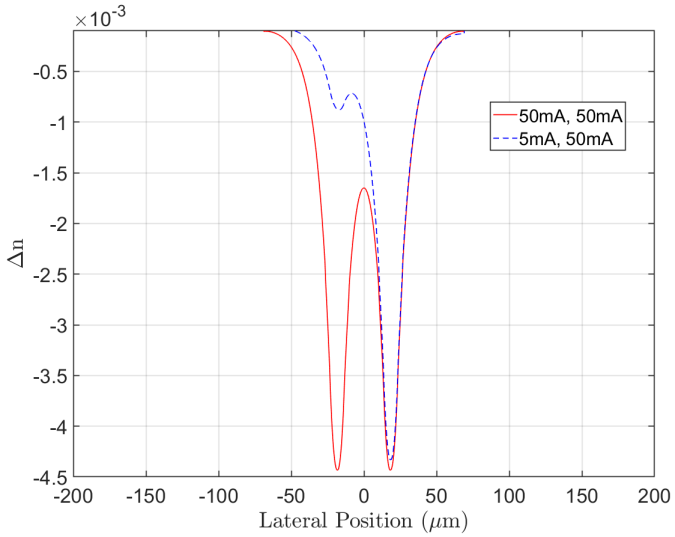

Figure 2. Cross section of the theoretical change in refractive index in the steering region of Sample A at 904nm under the contacts due to balanced (solid red line) and unbalanced (dashed blue line) current injection.

fibre coupling in optoelectronics packaging. The propagation loss of this curved waveguide due to its radius of curvature was calculated for each epitaxy using the tangential phase velocity method [17], and an appropriate radius of curvature chosen which resulted in an acceptable low loss for the device dimensions. Epitaxial growth parameters from previous work on polarisation maintaining, single mode waveguides at 780 nm [18], aided in the epitaxial designs of this work.

3. Optical & Electrical Characterisation

Characterisation of bare integrated optical components is challenging due to the high precision required to couple light into and out of the device, whilst ensuring minimal optical losses at the facets due to imperfect mode overlap between the mode of the input light and the waveguide. To characterise our devices, an optical test bench was designed and constructed to evaluate the performance of the switches over a range of parameters, such as insertion loss, extinction ratio, and switching speed. A schematic of this test bench is illustrated in Figure 3. Light from a 2mW laser diode is coupled into a x50 objective (Olympus LMPLFLN), mounted to a flexure stage with piezo actuators (Elliot Martock MDE125), facilitating precise adjustment of the size and position of the focused beam spot on the facet of the device. The device under test (DUT) is mounted on a gold plated, copper printed circuit board and bonded using gold ribbon and silver epoxy. This circuit board is mounted onto a machined aluminium plate, which is then mounted onto another flexure stage (Elliot Martock MDE123). An overhead microscope allows for plan view inspection of the device during alignment. The output light is collected by a x20 or x100 objective (Olympus MPLFLN) and the output facet of the device imaged using a CMOS camera. A variable gain photodetector is used to monitor the optical power level at the output facet. The DUT is controlled using a two-channel current source (Wavelength Electronics FL591). The current source is set using two separate digital to analogue converters (DACs), connected to a microcontroller (ESP32). Voltage levels are monitored using an FPGA (Red Pitaya).

Prior to mounting the switch for optical characterisation, the current density/voltage (J/V) response of the device structure was characterised using a probe station and source-measure unit (Keysight B2900A SMU). Results are shown in Figure 4. The ideality factors of Sample A and

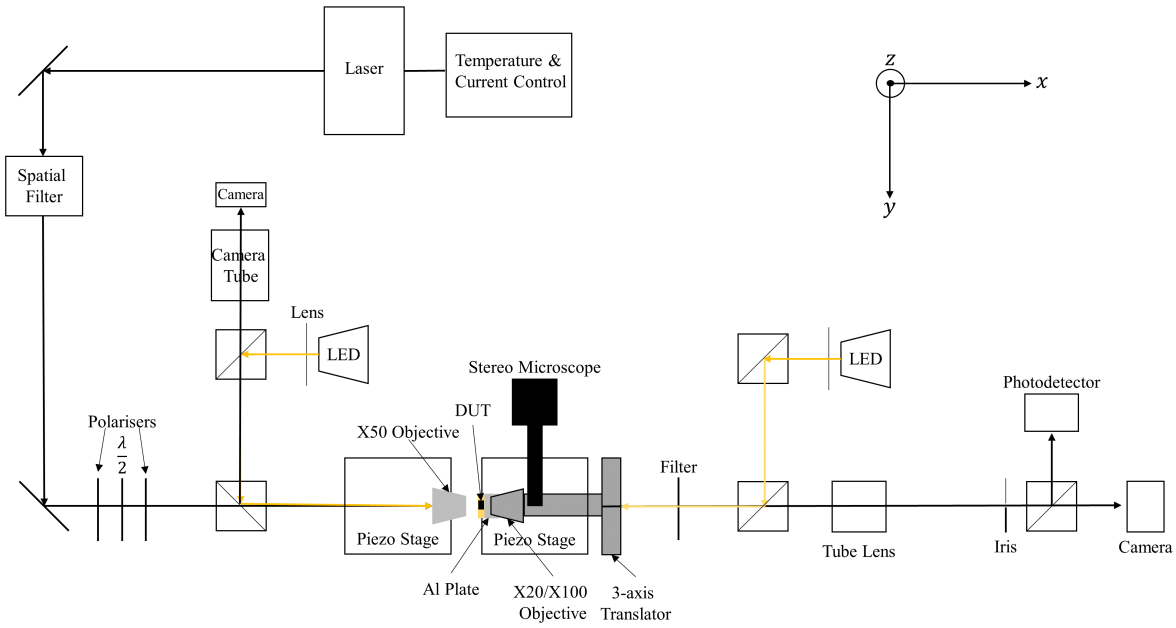

Figure 3. Schematic illustration of the optical test bench set-up used to characterise the optical switches. DUT = Device Under Test, LED = Light Emitting Diode

B at low bias ($0.8 \leq V \leq 1.5$) were evaluated and are summarised in Table 1. Characteristics for Sample C will be published elsewhere. The ideality factor measured at low bias voltages is determined by recombination currents in the depletion region and varies with the mesa diameter, whilst at higher voltages, the behaviour is dominated by the series resistance of the diode [19]. Ideality factors $\gg 1$ at low bias voltages can indicate issues with surface recombination and sidewall roughness, however these results confirm there are no such issues with these samples, and compare well with the literature for similar material/structure (see Table 1). The J/V characteristics also confirm that the electronic power requirements of these devices are sufficiently low and can be easily sourced by commercially available circuits for packaged optoelectronics. Rudimentary electrical switching tests were carried out using the probe station and source-measure unit (Keysight B2900A SMU) by switching each channel between 25 mA and 250mA. The observed upper limit on the rise and fall times of the optical switching is $\sim$120 μs [20]. The time response of the device is currently limited by the measurement equipment and does not represent the intrinsic switching speed of the devices.

The optical performance of Device A was tested by manually coupling 904 nm light into the input facet. By imaging the output facet, light was observed exiting the straight waveguide when the device was switched on and a small current ($\sim$5 mA) applied through both sets of contacts, as shown in Figure 5. This result indicated that the light entering the steering region was being steered into the straight waveguide, due to the channel waveguide formed by the injection of charge carriers. Using a lock-in detection method, the output light intensity at the straight waveguide was measured for a range of input currents, and the results illustrated in Figure 6. The lock-in detection was used to filter out any light generated by the device, by modulating the input laser light and detecting at only this frequency. This revealed that a maximum output intensity occurred with 12 mA through the right hand (RH) contact (in the direction of propagation) and 5 mA on the left hand (LH) contact. The current balance must

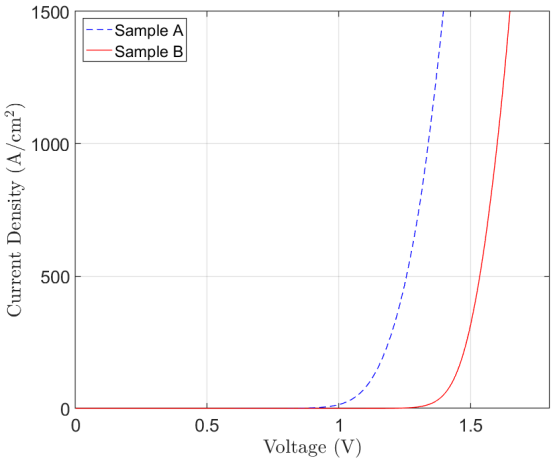

Figure 4. Current density/voltage characteristics, at $T = 300$ K, of p-i-n test structures for Sample A (blue dashed line) and Sample B (red solid line).

Table 1. Summary of the measured ideality factors of the p-i-n test devices and comparison to other work.

Reference	**Structure**	**Ideality Factor**
This Work (A)	$Al_{0.2}Ga_{0.8}As/GaAs/Al_{0.2}Ga_{0.8}As$	2.50 ± 0.10
This Work (B)	$Al_{0.45}Ga_{0.55}As/Al_{0.22}Ga_{0.78}As/Al_{0.45}Ga_{0.55}As$	1.72 ± 0.02
[19]	$Al_{0.4}Ga_{0.6}As/Al_{0.05}Ga_{0.95}As/Al_{0.4}Ga_{0.6}As$	1.74
[21]	$Al_{0.2}Ga_{0.8}As/GaAs/Al_{0.2}Ga_{0.8}As$	3.00 ± 0.28

be offset since the straight waveguide is offset from the centre of the device at the end of the steering region, as shown in Figure 7. The minimum output intensity occurred with 122 mA and 105 mA through the RH and LH contacts respectively. An extinction ratio of 13.4 dB was observed for this single device.

The intentional operation of the switch was that the curved waveguide should be used as the 'OFF' channel and the straight waveguide as the 'ON' channel. Initially, no light was observed exiting the output facet of the curved waveguide at any of the tested injection currents, indicating that the light had not propagated to the output facet. The extinction ratio was thus measured as a ratio of the maximum to the minimum output intensity at the output facet of the straight waveguide. In this instance, the beam was steered away from both waveguides and dispersed within the material. The map in Figure 6 contains interpolated data, however the extinction ratio was measured in relation to the actual recorded data. More recent testing with an automated coupling procedure has shown that it is possible to couple light into both waveguides simultaneously at low injection currents. More detailed results of these studies will be published at a later date. This recent finding confirms that initial measurements were limited by manual beam alignment.

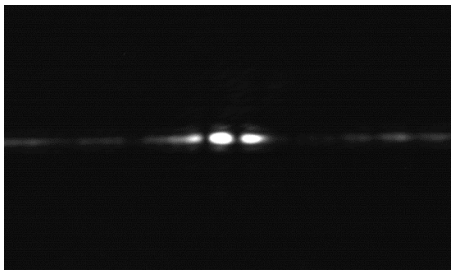

Figure 5. Image of light leaving the straight waveguide output facet of Device A with an injection 5 mA on each contact. The bright central spot indicates the position of the waveguide rib.

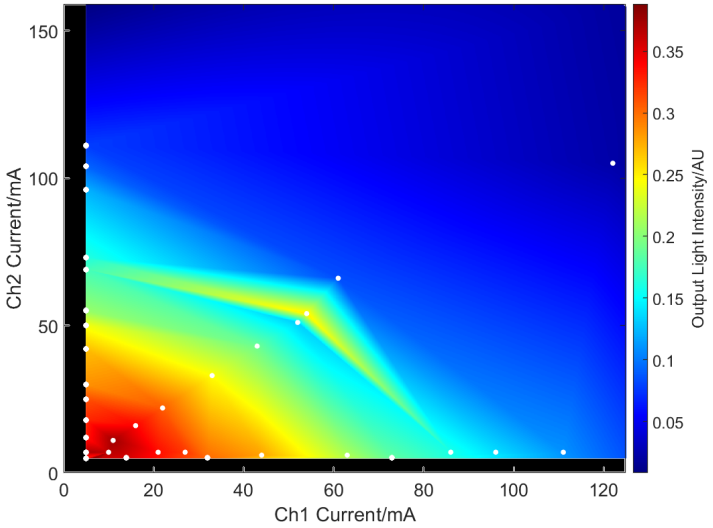

Figure 6. Interpolated map showing the output light intensity at the straight waveguide output facet of Device A for a range of electrical currents across each contact. The extinction ratio was calculated using measured data, with Ch1 = 5 mA, Ch2 = 12 mA as the 'ON' state and Ch1 = 122 mA, Ch2 = 105mA as the 'OFF' state. The white circles indicate measured data points.

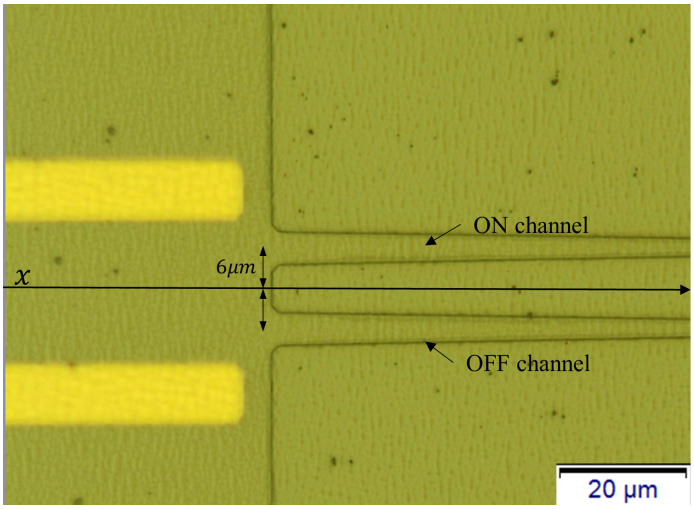

Figure 7. Optical micro-graph of Sample B during fabrication showing the position of the output waveguides at the end of the steering region. The tapered inputs to each waveguide are positioned 6 μm either side of the centre of the propagation (x) axis, requiring unbalanced currents to steer the beam into either channel.

4. Summary

We have presented a novel integrated semiconductor photonic switch design, based on carrier-induced refractive index change effects for use at near infrared wavelengths, intended for applications in quantum sensors. Initial testing of a device optimised for 890-920 nm revealed an extinction ratio of 13.4 dB, limited by manual beam alignment. An automated testing routine has since been developed and will be used to evaluate the performance of each optical switch design. Fabrication of devices designed for functionality in the wavelength ranges 750-780 nm and 745-775 nm is near completion and initial electrical characterisation has shown promising results.

Acknowledgements

We would like to thank the following people for their expertise and help during the project: Dr Andrew Rushforth and Dr Debi Pattnaik for help with ion beam milling, Mr Jasbinder Chauhan for his wealth of experience and advice with microfabrication, Mr Ian Taylor and Mr Andrew Stuart for their help with designing and implementing electronics and Mr Terry Wright for help with making device mounting hardware. We also wish to acknowledge project funding from the Engineering and Physical Sciences Research Council UK Quantum Technologies Hub for Sensors and Metrology, SM-30535, EP/M013294/1, and studentship funding EP/N509590/1.

References

[1] Hinton A, Perea-Ortiz M, Winch J, Briggs J, Freer S, Moustoukas D, Powell-Gill S, Squire C, Lamb A, Rammeloo C *et al.* 2017 *Philos. Trans. Royal Soc.* **375** 20160238
[2] Ménoret V, Vermeulen P, Le Moigne N, Bonvalot S, Bouyer P, Landragin A and Desruelle B 2018 *Sci. Rep.* **8** 1–11
[3] Zhou L, Long S, Tang B, Chen X, Gao F, Peng W, Duan W, Zhong J, Xiong Z, Wang J *et al.* 2015 *Phys. Rev. Lett.* **115** 013004
[4] Wicht A, Hensley J M, Sarajlic E and Chu S 2002 *Phys. Scr* **2002** 82
[5] Rosi G, Sorrentino F, Cacciapuoti L, Prevedelli M and Tino G M 2014 *Nature* **510** 518–21
[6] Hogan J M and Kasevich M A 2016 *Phys. Rev. A* **94** 033632
[7] Bongs K, Holynski M and Singh Y 2015 *Nat. Phys.* **11** 885–85
[8] Hauth M, Freier C, Schkolnik V, Senger A, Schmidt M and Peters A 2013 *Appl. Phys. B* **113** 49–55
[9] Bongs K, Malcolm Jand Ramelloo C, Zhu L, Boyer V, Valenzuela T, Maclean J, Piccardo-Selg A, Mellor C, Fernholz T *et al.* 2014 *Quantum Information and Measurement* (Optical Society of America) pp QTu3B–1
[10] Malcolm J I 2016 *Construction of a portable platform for cold atom interferometry* Ph.D. thesis University of Birmingham
[11] Kasevich M and Chu S 1992 *Appl. Phys. B* **54** 321–32
[12] Ravindran S, Datta A, Alameh K and Lee Y T 2012 *Opt. Express* **20** 15610–27
[13] Bennett B R, Soref R A and Del Alamo J A 1990 *IEEE J. Quantum Electron.* **26** 113–22
[14] Ferguson A, Kuver A, Heaton J, Zhou Y, Snowden C and Iezekiel S 2006 *IEE Proc. Optoelectron.* **153** 51–6
[15] Adachi S 1985 *J. Appl.* **58** R1–R29
[16] Ramaswamy V 1974 *Bell Syst. Tech. J.* **53** 697–704
[17] Marcatili E A J 1969 *Bell Syst. Tech. J.* **48** 2103–32
[18] Maclean J O, Greenaway M T, Campion R P, Pyragius T, Fromhold T M, Kent A J and Mellor C J 2014 *Integrated Optics: Devices, Materials, and Technologies XVIII* vol 8988 ed Broquin J E and Conti G N International Society for Optics and Photonics (Proc. SPIE) pp 19–28
[19] Corbett B and Kelly W M 1993 *Appl. Phys. Lett.* **62** 87–9
[20] Moss J L 2020 *Beam Steering Optical Switches in AlGaAs via the Burstein-Moss Effect* Ph.D. thesis University of Nottingham
[21] Dong X 2001 *Electrically-controlled optical beam steering and switching in semiconductor slab waveguide* Ph.D. thesis University of Central Florida